Sm-Nd isochron ages coupled with C-N isotope data of eclogitic diamonds from Jwaneng, Botswana

M.U. Gress, J.M. Koornneef, Emilie Thomassot, I.L. Chinn, K. van Zuilen, G.R. Davies

Journal Pre-proofs

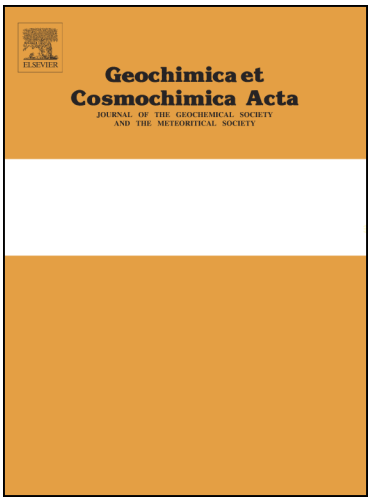

Sm-Nd isochron ages coupled with C-N isotope data of eclogitic diamonds from Jwaneng, Botswana

M.U. Gress, J.M. Koornneef, E. Thomassot, I.L. Chinn, K. van Zuilen, G.R. Davies

PII: S0016-7037(20)30642-6
DOI: https://doi.org/10.1016/j.gca.2020.10.010
Reference: GCA 11954

To appear in: *Geochimica et Cosmochimica Acta*

Received Date: 28 January 2020
Revised Date: 28 September 2020
Accepted Date: 8 October 2020

Please cite this article as: Gress, M.U., Koornneef, J.M., Thomassot, E., Chinn, I.L., van Zuilen, K., Davies, G.R., Sm-Nd isochron ages coupled with C-N isotope data of eclogitic diamonds from Jwaneng, Botswana, *Geochimica et Cosmochimica Acta* (2020), doi: https://doi.org/10.1016/j.gca.2020.10.010

Title

Sm-Nd isochron ages coupled with C-N isotope data of eclogitic diamonds from Jwaneng, Botswana

Authors

M.U. Gress[1,*], J.M. Koornneef[1], E. Thomassot[2,3], I.L. Chinn[4], K. van Zuilen[1], G.R. Davies[1]

[1] Vrije Universiteit, De Boelelaan 1085, 1081 HV Amsterdam, The Netherlands

[2] Université de Lorraine, Centre de Recherches Pétrographiques et Géochimiques (CRPG), 15 Rue Notre Dame des Pauvres, BP 20, 54 501 Vandœuvre-lès-Nancy, France

[3] Géosciences Montpellier, Université de Montpellier, CNRS, Université des Antilles, Montpellier, France.

[4] De Beers Exploration, Private Bag X01, Southdale 2135, South Africa

[*] Corresponding author. E-mail: m.u.gress@vu.nl

Abstract

Constraining the formation age of individual diamonds from incorporated mineral inclusions and assessing the host diamonds' geochemical characteristics allows determination of the complex history of diamond growth in the sub-continental lithospheric mantle (SCLM). It also provides the rare opportunity to study the evolution of the deep cycling of volatiles over time. To achieve these aims, Sm-Nd isotope systematics are presented for 36 eclogitic garnet and clinopyroxene inclusions from 16 diamonds from the Jwaneng mine, Botswana. The inclusions and host diamonds comprise at least two compositional suites that record different 'mechanisms' of diamond formation and define two

isochrons, one Paleoproterozoic (1.8 Ga) and one Neoproterozoic (0.85 Ga). There are indications of at least three additional diamond-forming events whose ages currently cannot be well constrained. The Paleoproterozoic diamond suite formed by large-scale (> 100's km), volatile-rich metasomatism related to formation and re-working of the Proto-Kalahari Craton. In contrast, the heterogeneous composition of the Neoproterozoic diamond suite indicates diamond formation on a small-scale, through local (< 10 km) equilibration of compositionally variable diamond-forming fluids in different eclogitic substrates during the progressive breakup of the Rodinia supercontinent. The results demonstrate that regional events appear to reflect the input of volatiles (i.e., carbon-bearing) derived from the asthenospheric mantle, whereas local diamond-forming events mainly promote the redistribution of volatiles within the SCLM. The occurrence of isotopically light carbon analysed in distinct growth zones from samples of this study ($\delta^{13}C$ < -21.1‰) provides further indication of a recycled origin for surface-derived carbon in some diamonds from Jwaneng. Determining Earth's long-term deep carbon cycle using diamonds, however, requires an understanding of the nature and scale of specific diamond-forming events.

Keywords

Diamond; Inclusion dating; Eclogite; Craton; Carbon and nitrogen isotope; Nitrogen aggregation

Word count ,

1. Introduction

Inclusions encapsulated in diamonds provide an unaltered record from Earth's otherwise inaccessible interior and information on the changing nature of Earth's deep carbon cycle. The Jwaneng mine in SE Botswana is Earth's richest diamond mine by value (Field et al., 2008) and provides samples that potentially constrain the temporal evolution and modification of the sub-continental lithospheric mantle

(SCLM) of the Archaean Kaapvaal Craton. Diamonds were transported to the surface during the eruption of the 235 ± 4 Ma Jwaneng kimberlites (Kinny et al., 1989) and notably, they are predominantly (up to 95%) of eclogitic (E-type) paragenesis, in comparison to the peridotitic (P-type) predominance worldwide (Stachel & Harris, 2008; Thomassot et al., 2009); an observation that appears characteristic of most diamond mines in Botswana (Gress et al., 2018; Timmerman et al., 2017) due to their craton-margin setting (Shirey et al., 2002) on the NW edge of the Kalahari Craton.

It is widely accepted that lithospheric diamonds and incorporated inclusions are of metasomatic origin and form in different substrates in the SCLM in the presence of volatile-rich liquids which are high-density C-H-O fluids or low degree melts at supra-solidus conditions (Deines, 1980; Schrauder et al., 1996; Sobolev et al., 2009; Sobolev et al., 1998; Stachel et al., 2005; Thomassot et al., 2007). Henceforth, the term fluid is used because distinction between the role of high density fluids and melts in diamond formation is difficult to resolve in gem-quality diamonds, which are the main focus of this study.

P-type diamonds formed in highly melt-depleted (harzburgitic) and lherzolitic substrates (Koornneef et al., 2017; Richardson et al., 1984). Eclogitic xenoliths suggest formation entirely within the SCLM (Griffin & O'Reilly, 2007; Hills & Haggerty, 1989; Smyth et al., 1989) or that the SCLM was infiltrated by melts derived from subducting oceanic lithosphere that retain strong geochemical records of its heterogeneity; i.e., hydrothermally altered lavas, dykes, gabbros, peridotite and chemical sediments (Aulbach et al., 2007; Aulbach & Jacob, 2016; Helmstaedt & Doig, 1975; Helmstaedt & Schulze, 1989; 2003; Jacob et al., 1994; MacGregor & Manton, 1986). In this context, sources for E-type diamonds have been widely ascribed to subduction of oceanic lithosphere and its incorporation into the peridotitic SCLM (Deines et al., 1984; Taylor et al., 1990) that experienced subsequent metasomatic overprint and partial melting (Sobolev et al., 1998; Taylor et al., 1996). In general, diamond-forming fluids are considered to modify the most incompatible elements of the eclogitic protolith, while compatible (e.g., major or high field-strength) elements still retain a signature of the protolith (Stachel et al., 2004). Websteritic (W-type) diamonds have a transitional character between P-/ E-type and their formation appears to be related to re-fertilisation reactions (Bodinier et al., 2008; Smit et al., 2014; Taylor et al., 2003) through mixing of mafic, possibly slab-derived, melts with

peridotitic SCLM (Aulbach et al., 2002) or wall-rock reactions in a plume setting (Sleep, 2006; Viljoen et al., 2018).

Cathodoluminescence studies coupled with various other spectroscopic properties of diamonds and inclusion populations reveal that most kimberlites contain multiple diamond populations (Boyd et al., 1987; Bulanova, 1995). Moreover, many individual diamonds record complex internal growth patterns with evidence of resorption events, marked zonation in nitrogen contents and a variety of carbon isotope ratios indicating the involvement of multiple, compositionally different diamond-forming fluids in their formation (Deines et al., 1984; Smart et al., 2011; Taylor et al., 1990; Wiggers de Vries et al., 2013). Recent dating studies of co-genetic silicate or sulphide inclusions using the Sm-Nd (Koornneef et al., 2017; Timmerman et al., 2017) and Re-Os isochron methods (Aulbach et al., 2009; Smit et al., 2016; Wiggers de Vries et al., 2013) verify several distinct periods of diamond formation.

1.1 Previous work on Jwaneng diamonds

Previous dating of eclogitic silicate inclusions from Jwaneng provided ^{40}Ar-^{39}Ar ages of clinopyroxenes (cpx) ranging from kimberlite eruption at 0.24 to 1.89 ± 0.45 Ga (Burgess et al., 1992). These results, however, are potentially compromised by radiogenic argon diffusion to the inclusion-diamond interface during mantle residence. Richardson et al. (1999) pooled 47 garnets (gnt) and 49 cpx from mono-mineralic inclusion-bearing diamonds to define a two-point Sm-Nd isochron age of 1.54 ± 0.02 Ga, with an initial ratio close to Bulk Earth (ε_{Nd} = +1.0). An individual large (> 1.1 mg) cpx inclusion from that study yielded a depleted mantle model age of ~1.0 Ga. Based on garnet major element and Sr isotope variations, the age was interpreted to potentially record mixing of two populations. This conclusion was supported by Re-Os isotope systematics of eclogitic sulphide inclusions that suggested possible diamond formation at ~ 2.9 Ga, ~ 1.5 Ga and potentially 2.1 Ga (Richardson et al., 2004). Additionally, previous studies on eclogitic silicate inclusion-bearing Jwaneng diamonds revealed a wide range in carbon ($\delta^{13}C$: -21.1‰ to -2.7‰) and nitrogen isotopes ($\delta^{15}N$: -10.1‰ to -1.1‰), N-content (0 to 1530 at.ppm) and N-aggregation (0 to 98 %B) and have been potentially mis-interpreted to record

primordial heterogeneity of the mantle (Deines et al., 1997) or to reflect a high-temperature fractionation process (Cartigny et al., 1998).

In addition, while robust isotopic evidence of recycled material has been reported on E-type sulphide inclusions at Jwaneng (non-zero $\Delta^{33}S$; Thomassot et al., 2009), no link to recycling of carbon and/ or nitrogen in their host diamonds has been identified. Instead, coupled C-N isotopes were interpreted to reflect mantle-related fluid evolution during diamond growth, due to as high temperature isotope fractionation (Cartigny et al., 1998; Thomassot et al., 2009). On the other hand, a significant proportion of eclogitic xenolith and inclusions in diamonds worldwide exhibit geochemical signatures of Earth's near surface such as Eu anomalies (Aulbach & Jacob, 2016; Jacob, 2004; Weiss et al., 2015), highly variable oxygen isotope ratios (Schulze et al., 2003; Sobolev et al., 2011) and MIF sulphur inherited from Archaean sediments (Chaussidon et al., 1987; Farquhar et al., 2002; Smit et al., 2019). Hence, the heterogeneity recorded in most eclogitic diamond suites raises fundamental questions about the processes that control diamond formation, in terms of timing, nature and scale, as well as the ultimate origin of the volatile elements in diamond-forming fluids in relation to the origin of incorporated inclusions (Bureau et al., 2018; Cartigny et al., 2014; Hogberg et al., 2016; Li et al., 2019). Moreover, dating of individual eclogitic silicate inclusions from discrete diamond growth zones, coupled with diamond and inclusion compositions allows inferences to be made about mechanisms of diamond formation and the regional scale on which it occurred.

2. Samples

The studied diamonds were selected from 130,000 diamonds based on optical identification of eclogitic inclusions. The inclusion positions were described in relation to the diamond growth structure (i.e., core, intermediate and rim growth zones) as listed in Table 1. Based on the isochronous nature of Sm-Nd results (Fig. 1), the inclusions were either assigned to groups (I to III) or labelled as 'unassigned', if no clear age relationships could be established. Inclusion compositions (see 4. Results) are in support

of this initial classification that is subsequently validated (see 5. Discussion). Henceforth, the inclusions with no isotope data are referred to as 'undated'.

The morphological characteristics, cathodoluminescence (CL) images and Fourier Transform Infrared Spectroscopy (FTIR) data from polished plates of the studied diamond hosts and a subset of major element compositions of the silicate inclusions were presented in full in Gress et al. (2018). The inclusion-bearing diamonds have a broad range of N content (≤ 20 – 839 at.ppm) and aggregation state (0 – 100 %B) and record either homogeneous growth with no detectable N or have systematic changes in N content from core to rim (for detailed traverses, see Appendix C.1). In combination with CL images, one (e.g., JW070; Fig. 2a), two (e.g., JW137, JW355; Fig. 2b,c) or three (e.g., JW147; Fig. 2d) growth events can be discerned within individual diamonds (Gress et al., 2018).

Samarium-Neodymium ages are reported from individual eclogitic garnet and cpx inclusions along with their major and trace element compositions and set in context with their corresponding diamond growth zones. Mineral inclusions from the same pool of Jwaneng diamonds from this study were identified as having characteristics indicative of both proto- (before) and syngenetic (at the same time) growth in relation to the diamond host (Davies et al., 2018). These authors found no evidence for the diamond lattice controlling the inclusions' growth directions (i.e., for epitaxial growth). At mantle temperatures, however, elemental diffusion between diamond-forming metasomatic fluids and protogenetic minerals about to be incorporated in the diamond would have been essentially instantaneous compared to the precision of the geochronology (Koornneef et al., 2017; Nestola et al., 2019; Taylor et al., 1996). Hence, in a geochronological context, the dated inclusions will record the time of diamond growth zone formation, i.e., they yield 'synchronous' ages.

3. Methods

Analytical details for the acquisition of major element compositions from the inclusions and data processing follow the protocol in Timmerman et al. (2015), clean-laboratory procedures are described

in Timmerman et al. (2017) and in Appendix A. Following chromatography, all matrix fractions were merged and dried down for trace element analyses on a Thermo X-Series II quadrupole ICP-MS. Samarium and neodymium isotope compositions were measured on a Thermo Scientific Triton *Plus* on four 10^{13} Ohm amplifiers. The isotopic ratios and elemental abundances were blank-corrected and include full propagation of uncertainties (Table 1); the blank uncorrected Sm-Nd and Rb-Sr data are provided in Table B.1.

Carbon isotopes of the major growth zones (sampled as fragments of about 0.05 – 0.1 mg from known locations within the diamond) were analysed by gas source mass spectrometry (31 diamonds) after combustion in an element analyser, as described in Timmerman et al. (2017) and in Appendix A. These analyses are referred to as 'combustion' and are expressed in delta notation relative to Vienna Pee Dee Belemnite (VPDB), $\delta^{13}C_{VPDB}$ [‰] = ($^{13}C/^{12}C_{sample}$ / $^{13}C/^{12}C_{PDB}$ - 1) x 10^3. Reported uncertainties in Table B.2 were obtained from the reference materials analysed in the corresponding analytical session and yield ± 0.16‰ (SD). In addition, we determined in-situ C-N isotopes and N content on polished diamond plates by SIMS, using a Cameca IMS-1280-HR2 multi-collection ion microprobe at CRPG-Nancy. This instrument has been recently upgraded with high sensitivity Faraday cups (FC's, 10^{12} Ω amplifiers), which are not subject to aging (unlike electron multipliers) and are easily cross-calibrated with other FC's. They significantly improve the statistical uncertainties associated with the collection of minor masses while working in multi-collection mode at high resolution. These data are referred to as 'SIMS' analyses. Carbon isotopes were measured during two independent analytical session, on central plates (n = 3 diamonds) in proximity of FTIR analyses and on polished fragments (n = 8 diamonds) obtained from major growth zones. Instrumental mass fractionation (IMF) was monitored using reference material (RM) Dp-418 ($\delta^{13}C$ = -5.32‰), Nam-56 ($\delta^{13}C$ = -29.3‰), Nam-114 ($\delta^{13}C$ = -26.93‰), see Cartigny et al. (2004), and give an absolute standard error of 0.14‰ for the entire analytical session. Long-term propagation (i.e. for the entire session) gives global uncertainties ranging from 0.29‰ to 0.33‰ (2SD). Overall, 25 duplicates and/ or triplicates of the same diamond growth zone were analysed in different sessions with indistinguishable results from the combustion analyses (Table B.2).

In-situ nitrogen content and isotopic composition were measured during a separate session, on polished fragments (n = 8) directly next to C isotope analysis location, on the same SIMS instrument with similar settings for the primary $^{133}Cs+$ beam (see Appendix A). The wide N concentration range of our RM collection (from 11 to 2740 at.ppm N; Appendix A) ensures a good calibration associated with small calibration error of ± 25 at.ppm (i.e. 5% error for a diamond containing 500 at.ppm). Nitrogen isotope data are expressed in delta notation relative to air, $\delta^{15}N_{AIR}$ [‰] = ($^{15}N/^{14}N_{sample}$ / $^{15}N/^{14}N_{AIR}$ - 1) x 10^3.

4. Results

Multiple inclusions from the same diamond (e.g., JW137 cpx A, B, D and garnet B) were labelled alphabetically. Two diamonds (JW336, JW346) contained silicate and sulphide inclusions, whilst the remainder had only silicate inclusions.

4.1 Carbon and nitrogen isotopic compositions of Jwaneng diamonds

Carbon isotope values from individual growth zones (n = 79) of 35 diamonds range from -23.2‰ to -1.4‰, with compositions from dated zones covering a more restricted range, -18.3‰ to -4.5‰. The dataset records a broadly bi-modal distribution (Fig. 3a) with C isotope compositions obtained from rims (together with a number of cores and intermediate zones) restricted to between -9.9‰ to -4.8‰, while several cores and one intermediate zone record lighter C isotope compositions (-23.2‰ to -18.2‰). In comparison, a more limited range has been reported from bulk stones and fragments of various diamond suites at Jwaneng (Cartigny et al., 1998; Deines et al., 1997; Thomassot et al., 2009). Traverses on JW060 and JW109 (Appendix C.1) show distinct N changes from core (JW060: 300 at.ppm, 80 %B; JW109: 100 at.ppm N, 55 %B) to rim (JW060: 480 at.ppm, 0 %B; JW109: 640 at.ppm N, 0 %B) with a narrow range in C isotope composition (JW060, $\delta^{13}C$: -6.7 to -4.3‰; JW109, $\delta^{13}C$: -

12.2 to -11.6‰). Nitrogen isotope values range from -4.7‰ to +5.8‰ (Fig. 3b) and SIMS-derived N abundances overlap with the FTIR data (Appendix C.1).

4.2 Cpx and garnet inclusion geochemistry

The major and trace element data of the cpx and garnet inclusions are reported in Table B.3. Cpx inclusions show a broad range in Mg# (molar 100*Mg/(Mg+Fe)) and Cr# (molar 100*Cr/(Cr+Al)) from 71 – 87 and 0 – 8, respectively (Fig. 4a) and classify as eclogitic and websteritic paragenesis. Following the nomenclature of Morimoto et al. (1988), the cpx are omphacite and augite with Na_2O ranging from 1.9 to 8.8 wt.%. Garnets (Fig. 4b) are pyrope-almandines with variable Mg# (45 – 80) and CaO (3.8 – 14.2 wt.%), but low Cr_2O_3 (≤ 0.5 wt.%). According to the updated classification scheme of Grütter et al. (2004), they fall in the eclogitic/ pyroxenitic/ websteritic (G4) and eclogitic (G3) compositional fields. Based solely on pyroxene inclusion chemistry, it is difficult to distinguish between a websteritic, clinopyroxenitic and orthopyroxenitic growth environment. For consistency with previous literature, we use the term websteritic paragenesis for diamonds JW047, JW355 and JW450 and eclogitic paragenesis for other samples. The E-type garnets can be further distinguished based on their Ca# (molar 100Ca/(Ca+Mn+Mg+Fe)) and Mg# into high-Ca (Ca# > 0.2; e.g., JW336, JW346, JW411) high-Mg (≥ 60; e.g., JW058, JW137, JW147 gnt E, JW355, JW450) and low-Mg (Mg# ≤ 60; JW175) as described in Aulbach & Jacob (2016).

The validity of the trace element compositions obtained from matrix residua (Fig. C.2) from the chromatography columns was confirmed by the bulk analysis of inclusions from the same diamond growth zones (JW058, JW070, JW147) that were too small (≤ 5 µg) for isotopic analysis. Cpx show a broad range in trace element ratios, e.g., Ba/Nb (2 – 2330) and have variable REE_N patterns (Fig. 5a) with some recording distinct changes of slope (kinks) with relative enrichment/ depletion in Ce, Pr and Nd. Garnets (Fig. 5b) are depleted in $LREE_N$ with $(Ce/Yb)_N < 0.7$, except for garnets of JW411 (2.0 – 2.4) and they also have a range of relative enrichment/ depletion in REE_N patterns. They have $(La/Nb)_N < 0.4$, except for garnets JW058 and JW411 (1.8). The cpx have 0.4 – 1 ppm Sm and 1 – 5.9 ppm Nd with $^{143}Nd/^{144}Nd$ of 0.5110 – 0.5132 and $^{147}Sm/^{144}Nd$ of 0.06 – 0.23. Garnets have 0.3 – 2.9 ppm Sm

and 0.5 – 5.8 ppm Nd with $^{143}Nd/^{144}Nd$ of 0.5120 – 0.5180 and $^{147}Sm/^{144}Nd$ of 0.12 – 0.7. The cpx have 44 – 253 ppm Sr and 0.1 – 36 ppm Rb with $^{87}Sr/^{86}Sr$ of 0.7026 – 0.7056 and $^{87}Rb/^{86}Sr$ of 0.001 – 1.38. Garnets have 1.1 – 9.8 ppm Sr and 0.04 – 0.7 ppm Rb with $^{87}Sr/^{86}Sr$ of 0.7061 – 0.7113 and $^{87}Rb/^{86}Sr$ of 0.04 – 1.8. Depleted mantle model ages (T_{DM}) were calculated using values from Michard et al. (1985) and range from 544 Ma to unrealistic ages older than Earth (Table 1) confirming a metasomatic, potentially multi-stage, evolution of the inclusions and thus, limiting their use to precisely define absolute age.

The mineral data obtained from inclusions within individual diamonds were filtered for evidence of disequilibrium between coexisting phases (Fig. 6a), as visible for example in JW147 that has disrupted light REE_N. The mineral REE_N partition coefficients ($D_{REE}^{cpx/gnt}$) are generally comparable with natural eclogitic inclusion pairs (Harte & Kirkley, 1997) and experimental data (Kessel et al., 2005; Klemme et al., 2002). Equilibration temperatures of non-touching garnet and cpx inclusion pairs from the same diamond growth zone (JW137, JW450) were calculated at 5 GPa using the thermometer of Ellis & Green (1979) T_{EG} and range from 1140°C – 1320°C (Table B.3). These temperatures are within uncertainty (±100°C; Stachel & Harris (2008)) of co-genetic, non-touching garnet-cpx inclusion pairs from Richardson et al. (1999) with T_{EG}: 1100°C – 1260°C. Theoretical REE_N patterns (Fig. 6b) were calculated for bulk rock eclogites to determine the nature of the inclusion protolith assuming an abundance of 45% cpx and 55% garnet, typical for mantle eclogites (Aulbach & Jacob, 2016).

5. Discussion

Ideally, an isochron is based on multiple mineral inclusions from the same growth zone of an individual diamond but such occurrences are exceptionally scarce because of complex growth histories. Only diamond JW137 (Fig. 2b) includes one high-Mg garnet and three augite inclusions (Sr_i = 0.704) in its rim (~ 55 at.ppm N; $\delta^{13}C$: -7.9‰ to -7.2‰) that yield a Sm-Nd isochron age of 911 ± 230 Ma with $^{143}Nd/^{144}Nd_i$= 0.51156 ± 0.00024 and ε_{Ndi} = +2.0. Several diamonds carry either multiple garnet

(JW411) or cpx inclusions (JW070, JW111, JW112, JW116, JW124) in the same growth zone that are within error of the isochrons and yield comparable initial ratios. Hence, it is necessary to assess the growth relationship of inclusions within the same and amongst different diamonds (Pearson et al., 1998) to prevent unintended mixing of different diamond populations. This problem was previously highlighted for two peridotitic diamond populations from Venetia (Koornneef et al., 2017) and is also obvious in the present data. Simply averaging the Sm-Nd data of all garnet (n = 13) and cpx (n = 23) inclusions in the study yields a composite isochron of 1395 ± 150 Ma with $^{143}Nd/^{144}Nd_i$= 0.51070 ± 0.00026 and ε_{Ndi}= -2.6. This age is within error of the two-point isochron age (1540 ± 20 Ma) of Richardson et al. (1999) determined on composites of 47 garnets and 49 cpx and confirms the authors' hypothesis that their data potentially record mixed populations (Fig. 1).

5.1 Determining the timing of diamond formation

Our data demonstrate multiple growth episodes at Jwaneng based on pairs of inclusions from different growth zones within individual diamonds. For example, JW336 garnet A (T_{DM} = 1110 Ma) from the inner core (90 at.ppm N; $\delta^{13}C$: -22.8‰), and garnet C (T_{DM} = 735 Ma) from the outer core (30 at.ppm N; $\delta^{13}C$: -18.3‰) have contrasting compositions. Similarly, JW058 garnet A (T_{DM} = 1708 Ma) from the core and cpx B (T_{DM} = 508 Ma) from the rim (N < 20 at.ppm N; $\delta^{13}C$ -8.2‰) or JW147 garnet E (intermediate zone; T_{DM} = 584 Ma; 290 at.ppm N, 54%B and $\delta^{13}C$: -4.0‰) and cpx A (core; T_{DM} = 1781 Ma; 106 at.ppm N and $\delta^{13}C$: -6.8‰) imply that the minerals are not co-genetic and represent different mineral populations. Hence, inclusion groups I to III (Fig. 1) are initially determined based on the Sm-Nd isotope data (Table. 1), which define at least two slopes on an isochron diagram (Fig. 1). Notably, inclusions from these three groups occur in separate diamonds and, except for inclusions from the unassigned group, no more than one inclusion group exists in any single diamond in this study implying spatially separate areas of diamond formation beneath Jwaneng. Given the compositional heterogeneity of the studied diamonds and their inclusions the data will be further assessed for genetic relationships.

Diffusion modelling (Nestola et al., 2019) indicates equilibration of Sm-Nd between inclusions (< 500 µm) and surrounding mantle must have occurred under diamond-forming conditions (T_{EG}: 1140°C – 1320°C of JW137, JW450) within millions of years. This is well within calculated uncertainties of the isochron precision (see below) validating that obtained ages in this study record the time of completed inclusion encapsulation inside the diamond and hence, the time of diamond formation.

5.1.1 Group I – 1791 ± 89 Ma (n= 16 inclusions)

Inclusions of group I consist of 14 augites (JW048, JW070, JW112, JW116, JW124) from five diamonds, all with relatively homogeneous high Cr# (2.6 to 4.7), high Mg# (80 to 87; Fig. 4a) and low Na_2O, (2.0 to 2.7 wt.%) and two pyrope almandines (JW058, JW346). Cpx inclusions have initial Sr isotope ratios ($^{87}Sr/^{86}Sr_i$), corrected to the inferred inclusion age, between 0.701 and 0.704, a limited range in $^{143}Nd/^{144}Nd$ ratios, from 0.5110 – 0.5116 (Table 1), relatively elevated Nd contents, from 2.7 to 5.9 ppm and low $^{147}Sm/^{144}Nd$ ratios of ≤ 0.11 (Fig. 1). They have marked $LREE_N$ enrichment ($(Ce/Yb)_N$ from 27 to 158) with sub-chondritic Lu (Fig. 5a) and Nb/La < 0.2. All these cpx inclusions have negative present-day ε_{Nd}, between -27 and -16 (Table 1) and although only indicative, T_{DM} ages are consistent and range from 1740 to 2050 Ma. The host growth zones are almost N-free (< 20 at.ppm) with a limited range in $\delta^{13}C$ (-8.5‰ to -6.4‰, Fig. 3, Table B.2). The garnets from JW346 ($^{87}Sr/^{86}Sr_i$ = 0.7069) and JW058 ($^{87}Sr/^{86}Sr_i$ = 0.7070) are $LREE_N$ depleted (Fig. 5b), with flat to increasing $MREE_N$ and flat, chondritic $HREE_N$ (JW058) or decreasing $HREE_N$ to subchondritic Lu (JW346) yielding a $(Ce/Yb)_N$ of 0.7 – 0.1. They have radiogenic $^{143}Nd/^{144}Nd$ of 0.5155 – 0.5180 and high $^{147}Sm/^{144}Nd$ of 0.43 – 0.65. Geochemical characteristics of the corresponding diamond growth zones are similar to the cpx-bearing diamonds with low N (JW058: core; < 20 at. ppm; JW346: intermediate; 192 at.ppm; 40 %B) and $\delta^{13}C$ of -8.7‰ to -8.2‰. Notably, both of these garnets define Nd T_{DM} ages of 1.7 Ga, suggesting a co-genetic relationship (Table B.2).

If only the cpx inclusions are considered, they define a Sm-Nd isochron age of 2078 ± 380 Ma (n = 14) with $^{143}Nd/^{144}Nd_i$= 0.51025 ± 0.00019 and ε_{Ndi}, +5.9. Including the co-genetic garnets JW346

(7.9 wt.% CaO) and JW058 (4.2 wt.% CaO) reduces the uncertainty in the isochron age to 1791 ± 89 Ma. Due to the marked $LREE_N$ enrichment of the sample suite, the initial ratio of $^{143}Nd/^{144}Nd_i = 0.51038 \pm 0.00006$, equivalent to $\varepsilon_{Ndi} = +1.3$, is consistent with derivation from a long-term mildly $LREE_N$-depleted source that became enriched in LREE immediately before or during diamond formation.

5.1.2 Group II – 853 ± 55 Ma (n = 11 inclusions)

Group II consists of 6 cpx and 5 garnet inclusions, including the four co-genetic inclusions in the rim of JW137. The inclusions that define the isochron are compositionally heterogeneous and include two high-Ca garnets ($^{87}Sr/^{86}Sr_i = 0.7054$) recovered from the intermediate zone of JW411 (~ 375 at.ppm N; $\delta^{13}C$: -5.0‰; $\delta^{15}N$: +5.2‰) with marked $LREE_N$ depletion and a negative slope in $MREE_N$–$HREE_N$ with sub-chondritic HREE abundances (Fig. 5b). Inclusions assigned to group II are two omphacites ($^{87}Sr/^{86}Sr_i = 0.7042$) of JW111 (core; 130 at.ppm N; $\delta^{13}C$: -11.2‰;) with a general $LREE_N$ enrichment peaking at Pr–Sm with a gradual decrease in $MREE_N$ and $HREE_N$ to chondritic Lu abundance (Fig. 5a). An omphacite ($^{87}Sr/^{86}Sr_i = 0.7044$) of JW138 (core; 60 at.ppm N; $\delta^{13}C$: -8.9‰) has a relative depletion in Pr–Nd, flat $MREE_N$ and decreasing $HREE_N$ to chondritic Lu. The high-Ca garnet C of JW336 (outer core; 30 at.ppm N; $\delta^{13}C$: -18.3‰) with a 'typical' eclogitic $LREE_N$ depleted pattern, with a steep positive slope and flat $MREE_N$–$HREE_N$, with REE compositions comparable to JW411 high-Ca garnets (Fig. 5b). JW147 E is a high-Mg garnet ($^{87}Sr/^{86}Sr_i = 0.7072$) with a REE_N pattern similar to JW137, with a $LREE_N$ depletion and flat $HREE_N$. Combined, these eleven inclusions from six diamonds define a diamond-forming event at 853 ± 55 Ma, with $^{143}Nd/^{144}Nd_i = 0.51167 \pm 0.0001$ and $\varepsilon_{Ndi} = +2.6$ (Fig. 1). The heterogeneous composition of group II inclusions implies the involvement of different components that will be critically addressed in the following sections.

5.1.3 Group III and unassigned diamonds – evidence for further events?

Five websteritic garnets (JW355, JW450; Fig. 2c) with have high Mg# (> 75) and low CaO (< 5.5 wt.%) are classified as group III. The garnets have $^{143}Nd/^{144}Nd$ between 0.5120 and 0.5125 below CHUR with restricted $^{147}Sm/^{144}Nd$ values close to chondritic (0.20 – 0.22), precluding reliable isochron or model

age determinations (Table 1). Diamond JW355 has a low N aggregation state (5 %B) associated with moderate N abundance (~ 570 at.ppm) and a typical mantle C isotope composition ($\delta^{13}C$: -4.6‰; $\delta^{15}N$: -4.0‰). Corresponding mantle residence temperatures (T_{MR}) were calculated according to Leahy & Taylor (1997). Such calculations are, however, only semi-quantitative at best. For example, it is impossible to resolve if some diamonds (e.g. JW450) were formed at 3.0 Ga and stored in the mantle on average at 1060°C or alternatively, diamond formation occurred immediately prior to kimberlite eruption (at 240 Ma) at 1120°C. The relatively flat REE_N patterns (Fig. 5b) with $(Ce/Yb)_N$ of 0.5 combined with the strongly unradiogenic $^{143}Nd/^{144}Nd$ values imply a multi-stage evolution with a time-integrated LREE-enriched source, either from a recycled crustal component or a LREE enriched component in SCLM, making it unlikely that group III inclusions and their hosts formed in the Archaean. There is currently no further evidence to constrain the time of formation of this diamond suite.

Four inclusions were unassigned to any group. The websteritic cpx (JW047) with a Cr# of 7.5, Mg# of 77.2 and 1.9 wt.% Na_2O is similar to group I compositions (< 20 at.ppm N; $\delta^{13}C$: -7.1‰) but has a distinct, unusually $MREE_N$-enriched pattern (Fig. 5a). Based on its Nd model age (T_{DM}: ~ 2930 Ma), the origin may be linked to diamond formation inferred for eclogitic sulphide inclusion-bearing diamonds at ~2.9 Ga (Richardson et al., 2004). However, currently, inclusion studies have provided no further evidence for silicate inclusion-bearing diamonds at Jwaneng of this age, although notably the garnet of JW346 (1.8 Ga isochron) was recovered from the intermediate zone and requires a prior event to form the diamond's core zone that incorporated a sulphide inclusion. The rim of the diamond host of JW058 cpx B (T_{DM} = 508 Ma) has < 20 at.ppm N and $\delta^{13}C$ of -8.2‰. The cpx has major element characteristics (Cr# of 3.0, Mg# of 82.1) similar to group I, but REE_N patterns similar to group II, ruling out a relationship to either group. Based on its Sm-Nd data and position in the inner core, $LREE_N$ depleted JW336 gnt A (T_{DM}: 1115 Ma) appears to belong to a distinct inclusion population that potentially formed chronologically between group I and II. There is evidence for diamond formation at 1.1 to 1.0 Ga across the Kalahari Craton (Koornneef et al., 2017; Timmerman et al., 2017).

While JW147 garnet (intermediate zone) can be unequivocally assigned to an isochron (group II), JW147 cpx (core) has a large uncertainty and a $^{143}Nd/^{144}Nd$ ratio close to CHUR that could potentially lie on either isochron. The cpx is therefore not assigned to an age group. Other undated diamonds provide evidence for discrete diamond-forming events with significant changes of N content and aggregation between adjacent growth zones with markedly different $\delta^{13}C$ composition e.g., JW397 (core: -21.2‰; rim: -9.9‰).

In conclusion, two separate diamond-forming events are identified in the mid-Paleoproterozoic (group I: 1791 ± 89 Ma) and mid-Neoproterozoic (group II: 853 ± 55 Ma) with additional diamond formation events suggested by other inclusions. The two populations have distinct characteristics. The older group I inclusions and their host diamonds have relatively homogeneous compositions, whereas the younger group II diamond and inclusion population has a compositional range. Importantly, however, inclusion pairs (e.g., JW111, JW137, JW411) validate the significance of the group II age.

5.2 The nature of the eclogitic environment of diamond formation

To constrain the nature and scale of the diamond-forming processes, we determined the parental fluids that formed garnet and cpx inclusions (Fig. C.3) and reconstructed bulk rock REE_N compositions (Fig. 6). The reconstructed bulk rock data for the three groups are distinct (Fig. 6b), with groups I and III being significantly LREE enriched (La_N: 26 – 40) with low HREE (Yb_N: 1 – 2), while group II is mildly LREE enriched (La_N: 14) with slightly elevated HREE (Yb_N: 4). The calculated bulk rocks are at the LREE-rich end of the range of eclogitic inclusions worldwide (Stachel et al., 2004) and resemble N-MORB protoliths that may have experienced loss of incompatible elements during subduction. Group I bulk rocks record the largest overall REE fractionation with $(Ce/Yb)_N$ ratios up to 8, compared to ratios of 5 in group III and 2 in the least fractionated group II .

Theoretical parental fluid compositions (Fig. C.3) for group I to III cpx and garnets were calculated using partitioning coefficients of hydrous experiments performed at 1000°C and 4 GPa from Kessel et al. (2005). These hypothetical fluids show a wide range of LREE enrichment (La_N = 15 – 1900 and $(Ce/Yb)_N$ = 45 – 2200) comparable to the range of compositions recorded in high density

fluids trapped in fibrous eclogitic diamonds from Jwaneng (Schrauder et al., 1996) and worldwide locations (Rege et al., 2010; Tomlinson & Müller, 2009; Weiss et al., 2013). These observations further support the hypothesis of common parental fluids for fibrous and gem-quality diamonds (Krebs et al., 2019).

5.2.1 Large-scale metasomatism (group I)

The compositional uniformity in group I diamonds (consistently low N contents, $\delta^{13}C$ from -8.7‰ to -6.4‰) and the homogeneous inclusion compositions recording only minor variation (e.g., $^{87}Sr/^{86}Sr_i$ ratios) establishes that large amounts of LREE enriched diamond-forming fluid (Fig. C.3) must have infiltrated eclogitic protoliths to initiate metasomatic diamond growth in the Paleoproterozoic. Together with mantle-like $\delta^{15}N$ (JW346 rim: -5.4‰), the uniform $\delta^{13}C$ possibly imply an asthenospheric origin for the diamond-forming fluid. Unfortunately, the absence of co-genetic garnet-cpx inclusion pairs within a diamond of group I do not allow for further insights as to the exact P/T conditions of formation. The large inferred fluid/rock ratio during diamond formation does, however, imply a large-scale geological process.

In this context it is noteworthy that a similar suite of low N (< 100 at.ppm) eclogitic diamonds from the Orapa kimberlite cluster 400 km NNE were also formed in the Paleo-Proterozoic (1.7 ± 0.3 Ga) and was interpreted to correspond to the amalgamation and breakup of the supercontinent Nuna/ Columbia (Timmerman et al., 2017). These diamonds have comparable $\delta^{13}C$ (-10.5‰ to -6.8‰) and relatively low $^{87}Sr/^{86}Sr_i$ suggesting a regional eclogitic diamond-forming event over length-scales of hundreds of kilometres. The age is also consistent with reworking of the SCLM beneath the NW margin of the Kalahari Craton (Fig. 7) during the amalgamation of the Kheis-Okwa-Magondi Belt and the Rehoboth Terrain between 2000 – 1750 Ma (Oriolo & Becker, 2018; Van Schijndel et al., 2011). This event has also been proposed to explain formation of diamonds with similar characteristics in Jagersfontein (Aulbach et al., 2009). These events were accompanied by subsequent rifting evolving northwards from the Kheis to the Magondi Belt and featured major rift-related volcanism (e.g., the Olifantshoek Volcanics or the Waterburg Lavas), plutonism (ultramafic to granitic) and regional

metamorphism (Hanson, 2003; McCourt et al., 2001) marking the final stage of the assembly of the Proto-Kalahari Craton (Jacobs et al., 2008).

5.2.2 Small-scale remobilization and local fluid equilibration (group II)

The eclogitic inclusions that define the group II isochron and their corresponding diamond growth zones ($\delta^{13}C$ from -18.3‰ to -4.0‰; JW147: $\delta^{15}N$ +1.9‰) are compositionally heterogeneous and therefore, suggest formation under low fluid/rock ratio conditions. Three augites (2.3 wt.% Na_2O) of JW137 (group II) show similar REE patterns and Mg# (79 to 80) to group I (except lower Cr#) and may imply a compositional but not a temporal relationship to group I inclusions. Notably, the co-genetic garnet and cpx inclusions of JW137 (Fig. 2b) validate the isochron age of group II. Despite the common Cr# < 1 (Fig. 4a), the remaining cpx of group II are omphacites (5.5 to 8.8 wt.% Na_2O).

Most group II inclusions are characterised by anomalous REE_N patterns (Fig. 5) with relative enrichment (JW111, JW137cpx) and depletion (JW138 cpx, JW147 gnt) in Ce_N–Nd_N. The abnormal REE_N patterns are not seen in samples of the older group I nor in other inclusion suites (Stachel et al., 2004). This atypical signature (also in JW147 cpx) is interpreted to reflect the involvement of REE-rich minor phases (e.g., apatite, barite, kyanite, rutile, zircon), either as crystallisation products from the metasomatic fluid or within the eclogitic protoliths. Such accessory phases act as a significant REE host in eclogites (Aulbach & Jacob, 2016). In addition, the large range of garnet CaO contents (4.2 – 14.2 wt.%) affects the partitioning of the REE (Aulbach & Jacob, 2016; Barth et al., 2001; Harte & Kirkley, 1997; O'Reilly & Griffin, 1995) and may explain the different $D_{REE}^{cpx/gnt}$ of the high-Ca garnets (12.6 – 12.9 wt.% CaO) from JW411 (Fig. 6b) that also has $(Nd/Er)_N > 1$ (Fig. 4b).

Overall, these variations are considered controlled by heterogeneity in the SCLM and suggest a more localised formation mechanism in comparison to group I. This conclusion is emphasised by the marked variation in T_{DM} ages of group II cpx and garnets (Table 1) and $^{87}Sr/^{86}Sr_i$ (0.7026 to 0.7071). Coupled with the potentially crustal $\delta^{15}N$ signature in JW147 (+1.9‰) and JW411 (+5.2‰), as well as the overall heterogeneous $\delta^{13}C$ (-18.3 ‰ to -4.0 ‰) of group II diamonds, this implies the potential involvement of different subducted components within the SCLM (Li et al., 2019). It seems unlikely,

however, that a single fluid, migrating and evolving through (different) protoliths, can account for the marked compositional heterogeneity of group II. It is considered more probably related to tectono-magmatic event(s) in which a series of low volumes of fluid interacted with spatially separate eclogitic protoliths. Remobilization/ infiltration of such diamond-forming fluids led to local equilibration with the SCLM (Giuliani et al., 2018) on a small-scale (< 10 km^3). Due to the limited $\delta^{15}N$ data it is impossible, however, to determine whether the fluids originated within the SCLM or whether they involved new subduction- or asthenosphere-derived sources that interact with heterogeneous SCLM. The precision of the isochron ultimately constrains the timescale of diamond formation to a period of < 100 millions of years.

The 0.85 Ga isochron age of group II diamond inclusions coincides with the breakup (Fig. 7) of the Rodinia supercontinent (900 – 700 Ma) that was accompanied by extensive evidence of rifting (e.g., in the Gariep Belt) and intra-plate magmatism (e.g., in the Magondi belt) along the NW and W margins of the Kalahari Craton (Ernst et al., 2008; Hanson, 2003; Jacobs et al., 2008). Currently, there are no comparable diamond formation ages reported from Botswana or western South Africa. This implies the responsible diamond forming event may not have metasomatised the SCLM beneath the NW edge of the Kalahari Craton on a regional scale. Alternatively, this age may not yet have been recognised as most reported dates are from inclusion composites. A possible explanation for the contrast with formation of group I diamonds is that following significant growth of the Kalahari Craton through Proterozoic accretion of micro-continents along its margins (Jacobs et al., 2008; Oriolo & Becker, 2018), the controlling tectono-magmatic event was significantly further away and led to limited fluid generation and heating of the regional SCLM beneath Jwaneng at 0.85 Ga (Fig. 7).

5.3 Implications for the deep carbon cycle

Diamond formation beneath Jwaneng involves large-scale (> 100's km) metasomatism with a high fluid/rock ratio forming group I samples and local (re-)mobilisation (< 10 km) of volatiles with a low fluid/rock ratio. To date, no diamonds that carry inclusions recording both events have been recognised possibly implying diamond formation in spatially separate parts of the SCLM beneath Jwaneng. These observations have significant implications for the constraints that can be placed on the deep carbon

cycle. The regional extent of the Paleoproterozoic inclusion suite together with its C-N isotope signature implies major addition of carbon from the asthenospheric mantle. A large-scale diamond-forming process with asthenosphere-derived fluids should overprint or dilute any existing signal derived from surface processes in the SCLM (Thomassot et al., 2009). In contrast, group II diamonds appear to record the local redistribution of carbon in the SCLM. As such, these latter diamonds do not provide quantitative information into the deep cycling of carbon but emphasise that there are multiple diamond populations present at Jwaneng that potentially have provided carbon of different origins for subsequent diamond formation. Evidence for the introduction of carbon into the SCLM at different times is provided by the presence of older generations of diamonds. This includes, group I and some of the unassigned diamonds from this study and distinct generations of sulphide-bearing diamonds recognised in the literature, some of which include a MIF sulphur isotope signature indicative > 2.5 Ga crustal recycling (Richardson et al., 2004; Thomassot et al., 2009).

The recognition of different mechanisms of diamond formation involving variable amounts and sources of carbon recycled within the SCLM may explain why it has been impossible so far to establish a consistent model for the deep carbon cycle through time (Shirey et al., 2019). Only events with large fluid/rock ratios will record the C isotope composition of material added to the SCLM. It is therefore important to fully understand the nature and scale of specific diamond formation events first.

6. Conclusions

Distinct eclogitic silicate inclusion populations at Jwaneng record multiple diamond-forming events. A large-scale event produced a relatively homogeneous suite of diamonds and silicate inclusions at 1790 ± 90 Ma that occur in the SCLM over large distances (> 500 km) beneath southern Africa. This event is related to Paleoproterozoic modifications of the Kalahari Craton under conditions characterised by a large fluid/rock ratio. Corresponding cpx have high Cr# (2.6 to 4.7), high Mg# (80 to 87), marked $LREE_N$ enrichment with $(Ce/Yb)_N$ from 27 to 158 to sub-chondritic Lu. The garnets have $LREE_N$

depletion with flat $MREE_N$ and $HREE_N$ depletion, diamond host growth zones have a narrow range in $\delta^{13}C$ (-8.7‰ to -6.4‰).

A second event occurred at 850 ± 55 Ma and is characterised by local (re-)mobilisation of fluids with an effective low fluid/rock ratio during the breakup of the Rodinia supercontinent resulting in a heterogeneous diamond suite. Corresponding cpx have low Cr# (< 1) and Mg# (71 to 80), garnets show a broad range in CaO (5.2 to 12.9 wt.%) and Mg# (45 to 75). All inclusions are characterised by anomalous REE_N patterns with relative enrichment or depletion in Ce_N–Nd_N and the host diamond growth zones have a broad range in $\delta^{13}C$ (-18.3‰ to -4.0‰) and $\delta^{15}N$ (+1.9‰).

The study also indicates additional events at ~ 3 Ga (JW047 cpx A, T_{DM} = 3192 Ma), at ~ 1 Ga (JW336 gnt A, T_{DM} = 1114 Ma) and potentially close to kimberlite eruption (group III). A previous published isochron age for Jwaneng diamond inclusions (1540 ± 20 Ma; Richardson et al. (1999)) is shown to be a consequence of mixing of multiple diamond populations. This result may have implications for the age reported for the Finch mine (1580 ± 50 Ma) 450 km to the SSW, which was also obtained from pooled inclusions (Richardson et al., 1999).

The multi-stage growth recorded in some individual Jwaneng diamonds that have inclusions of different age coupled with the presence of multiple diamond populations in general illustrates diamond formation is a recurring process throughout the evolution of Earth. On a global scale, the isochron ages overlap with a major (group I) and minor (group II) peaks in U-Pb zircon ages between 1800 – 2100 Ma and 750 – 900 Ma (Puetz, 2018), illustrating prominent episodes in continental crustal growth that are also witnessed by diamond inclusions (Shirey & Richardson, 2011). Although diamonds potentially document Earth's long-term deep carbon cycle, this study indicates that the nature and scale of specific diamond-forming events must be known before attempts can be made to constrain the nature of carbon exchange between deep and surficial reservoirs.

Acknowledgements

The authors sincerely thank Debswana and De Beers for providing access to run of mine production at DTCB and the generous supply of diamonds. MUG was funded through NWO project 824.14.004. Carbon isotope analyses were partly funded by Europlanet 2020 RI that received funding from the European Union's Horizon 2020 research and innovation programme under grant agreement No 654208. We thank Nordine Bouden for his technical assistance during SIMS analytical sessions as well as Etienne Deloule and Johan Villeneuve for the fruitful discussions while setting up the analytical condition for C-N isotope measurements by SIMS. Travel for sampling was sponsored by Stichting Dr. Schurmannfonds. Special thanks go to Hielke Jelsma for his advice on regional geology, Richard Smeets for assistance in the clean lab, to Pieter Ouwerkerk and Gassan Diamonds BV for assistance in polishing and to Suzan Verdegaal-Warmerdam, Ciaran Kelly, Evalien van der Valk and Anna Pals for their contributions in C isotope analyses. Sergei Matveev and Tilly Bouten are thanked for support with EPMA in Utrecht, Frank Peeters for providing access to the micro-balance and microscopy.

References

Aulbach S., Griffin W. L., Pearson N. J., O'Reilly S. Y. and Doyle B. J. (2007) Lithosphere formation in the central Slave Craton (Canada): plume subcretion or lithosphere accretion? *Contrib Mineral Petr* **154**(4): 409-427.

Aulbach S. and Jacob D. E. (2016) Major- and trace-elements in cratonic mantle eclogites and pyroxenites reveal heterogeneous sources and metamorphic processing of low-pressure protoliths. *Lithos* **262**: 586-605.

Aulbach S., Shirey S. B., Stachel T., Creighton S., Muehlenbachs K. and Harris J. W. (2009) Diamond formation episodes at the southern margin of the Kaapvaal Craton: Re–Os systematics of sulfide inclusions from the Jagersfontein Mine. *Contrib Mineral Petr* **157**(4): 525-540.

Aulbach S., Stachel T., Viljoen S. K., Brey G. P. and Harris J. W. (2002) Eclogitic and websteritic diamond sources beneath the Limpopo Belt–is slab-melting the link? *Contrib Mineral Petr* **143**(1): 56-70.

Barth M. G., Rudnick R. L., Horn I., McDonough W. F., Spicuzza M. J., Valley J. W. and Haggerty S. E. (2001) Geochemistry of xenolithic eclogites from West Africa, Part I: a link between low MgO eclogites and Archean crust formation. *Geochim Cosmochim Ac* **65**(9): 1499-1527.

Bodinier J.-L., Garrido C. J., Chanefo I., Bruguier O. and Gervilla F. (2008) Origin of pyroxenite–peridotite veined mantle by refertilization reactions: evidence from the Ronda peridotite (Southern Spain). *Journal of Petrology* **49**(5): 999-1025.

Boyd S., Mattey D., Pillinger C., Milledge H., Mendelssohn M. and Seal M. (1987) Multiple growth events during diamond genesis: an integrated study of carbon and nitrogen isotopes and nitrogen aggregation state in coated stones. *Earth Planet Sc Lett* **86**(2-4): 341-353.

Bulanova G. (1995) The formation of diamond. *J Geochem Explor* **53**(1): 1-23.

Bureau H., Remusat L., Esteve I., Pinti D. L. and Cartigny P. (2018) The growth of lithospheric diamonds. *Science Advances* **4**(6): eaat1602.

Burgess R., Turner G. and Harris J. (1992) 40Ar-39Ar laser probe studies of clinopyroxene inclusions in eclogitic diamonds. *Geochim Cosmochim Ac* **56**(1): 389-402.

Cartigny P., Harris J. W. and Javoy M. (1998) Eclogitic Diamond Formation at Jwaneng: No Room for a Recycled Component. *Science* **280**(5368): 1421-1424.

Cartigny P., Palot M., Thomassot E. and Harris J. W. (2014) Diamond formation: a stable isotope perspective. *Annual Review of Earth and Planetary Sciences* **42**: 699-732.

Cartigny P., Stachel T., Harris J. W. and Javoy M. (2004) Constraining diamond metasomatic growth using C-and N-stable isotopes: examples from Namibia. *Lithos* **77**(1): 359-373.

Chaussidon M., Albarede F. and Sheppard S. (1987) Sulphur isotope heterogeneity in the mantle from ion microprobe measurements of sulphide inclusions in diamonds. *Nature* **330**(6145): 242-244.

Davies G. R., van den Heuvel Q., Matveev S., Drury M. R., Chinn I. L. and Gress M. U. (2018) A combined cathodoluminescence and electron backscatter diffraction examination of the growth

relationships between Jwaneng diamonds and their eclogitic inclusions. *Mineralogy and Petrology* **112**(1): 231-242.

Deines P. (1980) The carbon isotopic composition of diamonds: relationship to diamond shape, color, occurrence and vapor composition. *Geochim Cosmochim Ac* **44**(7): 943-961.

Deines P., Gurney J. J. and Harris J. W. (1984) Associated chemical and carbon isotopic composition variations in diamonds from Finsch and Premier kimberlite, South Africa. *Geochim Cosmochim Ac* **48**(2): 325-342.

Deines P., Harris J. and Gurney J. (1997) Carbon isotope ratios, nitrogen content and aggregation state, and inclusion chemistry of diamonds from Jwaneng, Botswana. *Geochim Cosmochim Ac* **61**(18): 3993-4005.

Ellis D. and Green D. (1979) An experimental study of the effect of Ca upon garnet-clinopyroxene Fe-Mg exchange equilibria. *Contrib Mineral Petr* **71**(1): 13-22.

Ernst R., Wingate M., Buchan K. and Li Z.-X. (2008) Global record of 1600–700 Ma Large Igneous Provinces (LIPs): implications for the reconstruction of the proposed Nuna (Columbia) and Rodinia supercontinents. *Precambrian Research* **160**(1-2): 159-178.

Farquhar J., Wing B., McKeegan K., Harris J., Cartigny P. and Thiemens M. (2002) Mass-independent sulfur of inclusions in diamond and sulfur recycling on early Earth. *Science* **298**(5602): 2369-2372.

Field M., Stiefenhofer J., Robey J. and Kurszlaukis S. (2008) Kimberlite-hosted diamond deposits of southern Africa: A review. *Ore Geol Rev* **34**(1–2): 33-75.

Giuliani A., Woodhead J. D., Phillips D., Maas R., Davies G. R. and Griffin W. L. (2018) Titanates of the lindsleyite–mathiasite (LIMA) group reveal isotope disequilibrium associated with metasomatism in the mantle beneath Kimberley (South Africa). *Earth Planet Sc Lett* **482**: 253-264.

Gress M. U., Howell D., Chinn I. L., Speich L., Kohn S. C., van den Heuvel Q., Schulten E., Pals A. S. and Davies G. R. (2018) Episodic diamond growth beneath the Kaapvaal Craton at Jwaneng Mine, Botswana. *Mineralogy and Petrology* **112**(1): 219-229.

Griffin W. L. and O'Reilly S. Y. (2007) Cratonic lithospheric mantle: is anything subducted? *Episodes* **30**(1): 43-53.

Grütter H. S., Gurney J. J., Menzies A. H. and Winter F. (2004) An updated classification scheme for mantle-derived garnet, for use by diamond explorers. *Lithos* **77**(1): 841-857.

Hanson R. (2003) Proterozoic geochronology and tectonic evolution of southern Africa. *Geological Society, London, Special Publications* **206**(1): 427-463.

Harte B. and Kirkley M. B. (1997) Partitioning of trace elements between clinopyroxene and garnet: data from mantle eclogites. *Chemical Geology* **136**(1): 1-24.

Helmstaedt H. and Doig R. (1975) Eclogite nodules from kimberlite pipes of the Colorado Plateau—samples of subducted Franciscan-type oceanic lithosphere. *Physics and Chemistry of the Earth*, Elsevier**:** 95-111.

Helmstaedt H. and Schulze D. (1989) Southern African kimberlites and their mantle sample: implications for Archean tectonics and lithosphere evolution. *Kimberlites and related rocks* **1**: 358-368.

Hills D. V. and Haggerty S. E. (1989) Petrochemistry of eclogites from the Koidu kimberlite complex, Sierra Leone. *Contrib Mineral Petr* **103**(4): 397-422.

Hogberg K., Stachel T. and Stern R. A. (2016) Carbon and nitrogen isotope systematics in diamond: Different sensitivities to isotopic fractionation or a decoupled origin? *Lithos* **265**: 16-30.

Jacob D. E. (2004) Nature and origin of eclogite xenoliths from kimberlites. *Lithos* **77**(1): 295-316.

Jacob D. E., Fung A., Jagoutz E. and Pearson D. G. (2003) *Petrology and geochemistry of eclogite xenoliths from the Ekati kimberlites area*. International Kimberlite Conference: Extended Abstracts.

Jacob D. E., Jagoutz E., Lowry D., Mattey D. and Kudrjavtseva G. (1994) Diamondiferous eclogites from Siberia: remnants of Archean oceanic crust. *Geochim Cosmochim Ac* **58**(23): 5191-5207.

Jacobs J., Pisarevsky S., Thomas R. J. and Becker T. (2008) The Kalahari Craton during the assembly and dispersal of Rodinia. *Precambrian Research* **160**(1-2): 142-158.

Kessel R., Schmidt M. W., Ulmer P. and Pettke T. (2005) Trace element signature of subduction-zone fluids, melts and supercritical liquids at 120–180 km depth. *Nature* **437**(7059): 724.

Kinny P., Compston W., Bristow J. and Williams I. (1989) Archaean mantle xenocrysts in a Permian kimberlite: two generations of kimberlitic zircon in Jwaneng DK2, southern Botswana. *Kimberlites and Related Rocks* **2**: 833-842.

Klemme S., Blundy J. D. and Wood B. J. (2002) Experimental constraints on major and trace element partitioning during partial melting of eclogite. *Geochim Cosmochim Ac* **66**(17): 3109-3123.

Koornneef J. M., Gress M. U., Chinn I. L., Jelsma H. A., Harris J. W. and Davies G. R. (2017) Archaean and Proterozoic diamond growth from contrasting styles of large-scale magmatism. *Nat Commun* **8**(1): 648.

Krebs M., Pearson D., Stachel T., Laiginhas F., Woodland S., Chinn I. and Kong J. (2019) A common parentage-low abundance trace element data of gem diamonds reveals similar fluids to fibrous diamonds. *Lithos* **324**: 356-370.

Leahy K. and Taylor W. (1997) The influence of the Glennie domain deep structure on the diamonds in Saskatchewan kimberlites. *Geol Geofiz* **38**(2): 451-460.

Li K., Li L., Pearson D. G. and Stachel T. (2019) Diamond isotope compositions indicate altered igneous oceanic crust dominates deep carbon recycling. *Earth Planet Sc Lett* **516**: 190-201.

MacGregor I. D. and Manton W. I. (1986) Roberts Victor eclogites: ancient oceanic crust. *Journal of Geophysical Research: Solid Earth* **91**(B14): 14063-14079.

McCourt S., Hilliard P., Armstrong R. and Munyanyiwa H. (2001) SHRIMP U-Pb zircon geochronology of the Hurungwe granite northwest Zimbabwe: Age constraints on the timing of the Magondi orogeny and implications for the correlation between the Kheis and Magondi Belts. *South African Journal of Geology* **104**(1): 39-46.

Michard A., Gurriet P., Soudant M. and Albarede F. (1985) Nd isotopes in French Phanerozoic shales: external vs. internal aspects of crustal evolution. *Geochim Cosmochim Ac* **49**(2): 601-610.

Morimoto N., Fabries J., Ferguson A. K., Ginzburg I. V., Ross M., Seifert F. A., Zussman J., Aoki K. and Gottardi G. (1988) Nomenclature of pyroxenes. *American Mineralogist* **73**(9-10): 1123-1133.

Nestola F., Jacob D. E., Pamato M. G., Pasqualetto L., Oliveira B., Greene S., Perritt S., Chinn I., Milani S., Kueter N., Sgreva N., Nimis P., Secco L. and Harris J. W. (2019) Protogenetic garnet inclusions and the age of diamonds. *Geology* **47**(5): 431-434.

O'Reilly S. Y. and Griffin W. (1995) Trace-element partitioning between garnet and clinopyroxene in mantle-derived pyroxenites and eclogites: PTX controls. *Chemical Geology* **121**(1-4): 105-130.

Oriolo S. and Becker T. (2018) The Kalahari Craton, Southern Africa: from Archean crustal evolution to Gondwana amalgamation. *Geology of Southwest Gondwana*, Springer**:** 133-159.

Pearson D. G., Shirey S., Harris J. and Carlson R. (1998) Sulphide inclusions in diamonds from the Koffiefontein kimberlite, S Africa: constraints on diamond ages and mantle Re–Os systematics. *Earth Planet Sc Lett* **160**(3): 311-326.

Puetz S. J. (2018) A relational database of global U–Pb ages. *Geoscience Frontiers* **9**(3): 877-891.

Rege S., Griffin W. L., Pearson N., Araújo D., Zedgenizov D. and O'Reilly S. Y. (2010) Trace-element patterns of fibrous and monocrystalline diamonds: insights into mantle fluids. *Lithos* **118**(3): 313-337.

Richardson S. H., Chinn I. L. and Harris J. W. (1999) Age and origin of eclogitic diamonds from the Jwaneng kimberlite, Botswana. *The PH Nixon Volume Proceedings of the Seventh International Kimberlite Conference,Cape Town. Red Roof Design, Cape Town,*: 734-736.

Richardson S. H., Gurney J. J., Erlank A. J. and Harris J. W. (1984) Origin of diamonds in old enriched mantle. *Nature* **310**(5974): 198-202.

Richardson S. H., Shirey S. B. and Harris J. W. (2004) Episodic diamond genesis at Jwaneng, Botswana, and implications for Kaapvaal craton evolution. *Lithos* **77**(1–4): 143-154.

Schrauder M., Koeberl C. and Navon O. (1996) Trace element analyses of fluid-bearing diamonds from Jwaneng, Botswana. *Geochim Cosmochim Ac* **60**(23): 4711-4724.

Schulze D. J., Harte B., Valley J. W., Brenan J. M. and Dominic M. D. R. (2003) Extreme crustal oxygen isotope signatures preserved in coesite in diamond. *Nature* **423**(6935): 68-70.

Shirey S. B., Harris J. W., Richardson S. H., Fouch M. J., James D. E., Cartigny P., Deines P. and Viljoen F. (2002) Diamond genesis, seismic structure, and evolution of the Kaapvaal-Zimbabwe craton. *Science* **297**(5587): 1683-1686.

Shirey S. B. and Richardson S. H. (2011) Start of the Wilson Cycle at 3 Ga Shown by Diamonds from Subcontinental Mantle. *Science* **333**(6041): 434-436.

Shirey S. B., Smit K., Pearson D. G., Walter M., Aulbach S., Brenker F., Bureau H., Burnham A., Cartigny P. and Chacko T. (2019) Diamonds and the Mantle Geodynamics of Carbon. *Deep carbon*.

Sleep N. H. (2006) Mantle plumes from top to bottom. *Earth-Science Reviews* **77**(4): 231-271.

Smart K. A., Chacko T., Stachel T., Muehlenbachs K., Stern R. A. and Heaman L. M. (2011) Diamond growth from oxidized carbon sources beneath the Northern Slave Craton, Canada: a δ 13 C–N study of eclogite-hosted diamonds from the Jericho kimberlite. *Geochim Cosmochim Ac* **75**(20): 6027-6047.

Smit K. V., Pearson D. G., Stachel T. and Seller M. (2014) Peridotites from Attawapiskat, Canada: Mesoproterozoic reworking of palaeoarchaean lithospheric mantle beneath the northern superior superterrane. *Journal of Petrology* **55**(9): 1829-1863.

Smit K. V., Shirey S. B., Hauri E. H. and Stern R. A. (2019) Sulfur isotopes in diamonds reveal differences in continent construction. *Science* **364**(6438): 383-385.

Smit K. V., Shirey S. B. and Wang W. (2016) Type Ib diamond formation and preservation in the West African lithospheric mantle: Re–Os age constraints from sulphide inclusions in Zimmi diamonds. *Precambrian Research* **286**: 152-166.

Smit K. V., Stachel T., Luth R. W. and Stern R. A. (2019) Evaluating mechanisms for eclogitic diamond growth: An example from Zimmi Neoproterozoic diamonds (West African craton). *Chemical Geology* **520**: 21-32.

Smyth J. R., Caporuscio F. A. and McCormick T. C. (1989) Mantle eclogites: evidence of igneous fractionation in the mantle. *Earth Planet Sc Lett* **93**(1): 133-141.

Sobolev N., Logvinova A. and Efimova E. (2009) Syngenetic phlogopite inclusions in kimberlite-hosted diamonds: implications for role of volatiles in diamond formation. *Russian Geology and Geophysics* **50**(12): 1234-1248.

Sobolev N., Schertl H.-P., Valley J. W., Page F., Kita N. T., Spicuzza M. J., Neuser R. and Logvinova A. (2011) Oxygen isotope variations of garnets and clinopyroxenes in a layered diamondiferous calcsilicate rock from Kokchetav Massif, Kazakhstan: a window into the geochemical nature of deeply subducted UHPM rocks. *Contrib Mineral Petr* **162**(5): 1079.

Sobolev N., Snyder G. A., Taylor L. A., Keller R. A., Yefimova E. S., Sobolev V. N. and Shimizu N. (1998) Extreme chemical diversity in the mantle during eclogitic diamond formation: evidence from 35 garnet and 5 pyroxene inclusions in a single diamond. *International Geology Review* **40**(7): 567-578.

Stachel T., Aulbach S., Brey G. P., Harris J. W., Leost I., Tappert R. and Viljoen K. F. (2004) The trace element composition of silicate inclusions in diamonds: a review. *Lithos* **77**(1-4): 1-19.

Stachel T., Brey G. P. and Harris J. W. (2005) Inclusions in sublithospheric diamonds: glimpses of deep Earth. *Elements* **1**(2): 73-78.

Stachel T. and Harris J. W. (2008) The origin of cratonic diamonds—constraints from mineral inclusions. *Ore Geol Rev* **34**(1): 5-32.

Stachel T., Viljoen K., McDade P. and Harris J. (2004) Diamondiferous lithospheric roots along the western margin of the Kalahari Craton—the peridotitic inclusion suite in diamonds from Orapa and Jwaneng. *Contrib Mineral Petr* **147**(1): 32-47.

Taylor L. A., Anand M. and Promprated P. (2003) *Diamonds and their inclusions: are the criteria for syngenesis valid*. 8th International Kimberlite Conference. Long Abstract, Victoria, Canada.

Taylor L. A., Snyder G. A., Crozaz G., Sobolev V. N., Yefimova E. S. and Sobolev N. V. (1996) Eclogitic inclusions in diamonds: evidence of complex mantle processes over time. *Earth Planet Sc Lett* **142**(3): 535-551.

Taylor W., Jaques A. and Ridd M. (1990) Nitrogen-defect aggregation characteristics of some Australasian diamonds: time-temperature constraints on the source regions of pipe and alluvial diamonds. *American Mineralogist* **75**: 1290-1310.

Thomassot E., Cartigny P., Harris J., Lorand J., Rollion-Bard C. and Chaussidon M. (2009) Metasomatic diamond growth: A multi-isotope study (13 C, 15 N, 33 S, 34 S) of sulphide inclusions and their host diamonds from Jwaneng (Botswana). *Earth Planet Sc Lett* **282**(1): 79-90.

Thomassot E., Cartigny P., Harris J. and Viljoen K. F. (2007) Methane-related diamond crystallization in the Earth's mantle: stable isotope evidences from a single diamond-bearing xenolith. *Earth Planet Sc Lett* **257**(3): 362-371.

Timmerman S., Koornneef J. M., Chinn I. L. and Davies G. R. (2017) Dated eclogitic diamond growth zones reveal variable recycling of crustal carbon through time. *Earth Planet Sc Lett* **463**: 178-188.

Timmerman S., Matveev S., Gress M. U. and Davies G. R. (2015) A methodology for wavelength dispersive electron probe microanalysis of unpolished silicate minerals. *J Geochem Explor* **159**(Supplement C): 243-251.

Tomlinson E. and Müller W. (2009) A snapshot of mantle metasomatism: trace element analysis of coexisting fluid (LA-ICP-MS) and silicate (SIMS) inclusions in fibrous diamonds. *Earth Planet Sc Lett* **279**(3-4): 362-372.

Van Schijndel V., Cornell D. H., Hoffmann K.-H. and Frei D. (2011) Three episodes of crustal development in the Rehoboth Province, Namibia. *Geological Society, London, Special Publications* **357**(1): 27-47.

Viljoen K., Perritt S. and Chinn I. (2018) An unusual suite of eclogitic, websteritic and transitional websteritic-lherzolitic diamonds from the Voorspoed kimberlite in South Africa: Mineral inclusions and infrared characteristics. *Lithos* **320**: 416-434.

Weiss Y., Griffin W. and Navon O. (2013) Diamond-forming fluids in fibrous diamonds: the trace-element perspective. *Earth Planet Sc Lett* **376**: 110-125.

Weiss Y., McNeill J., Pearson D. G., Nowell G. M. and Ottley C. J. (2015) Highly saline fluids from a subducting slab as the source for fluid-rich diamonds. *Nature* **524**(7565): 339-342.

Wiggers de Vries D., Bulanova G., De Corte K., Pearson D., Craven J. and Davies G. (2013) Micron-scale coupled carbon isotope and nitrogen abundance variations in diamonds: Evidence for episodic diamond formation beneath the Siberian Craton. *Geochim Cosmochim Ac* **100**: 176-199.

Wiggers de Vries D., Pearson D. G., Bulanova G., Smelov A., Pavlushin A. and Davies G. (2013) Re–Os dating of sulphide inclusions zonally distributed in single Yakutian diamonds: evidence for multiple episodes of Proterozoic formation and protracted timescales of diamond growth. *Geochim Cosmochim Ac* **120**: 363-394.

Tables

Table 1: Sm-Nd data of eclogitic silicate inclusions from Jwaneng.

Figures

Figure 1: Sm-Nd isochrons for group I (red; 1791 ± 89 Ma with ε_{Nd_i} = +1.3) and group II (green; 853 ± 55 Ma with ε_{Nd_i} = +2.6) compared to the composite 1.54 Ga isochron age of Richardson et al. (1999) that records mixing of different inclusion populations. Individual diamond inclusions from Orapa (400 km north) that lie on a 1.69 Ga isochron (Timmerman et al., 2017) are interpreted to have formed during the same large-scale event that formed Group I samples. Inclusions of group III (purple) and those unassigned to a group (blue) emphasise the complexity of diamond formation at Jwaneng.

Figure 2: Representative diamonds with light microscope- and CL-images indicating the relative location of studied garnet (square) and cpx (circle) inclusions annotated by: group I to III, unassigned (u) and undated (empty symbols). Note: symbol size corresponds to relative size of the inclusion; stippled line indicates inclusions recovered from the offcut, solid line from the plate. a) JW070 (group I): no clear growth zonation recognisable with green slip lines indicating deformation; b) JW137 (group II): resorption at the core-rim interface and deformation indicated in the rim; c) JW355 (group III): the overall low N aggregation makes it difficult to clearly distinguish between core-rim. d) JW147: note the different CL characteristics of the intermediate zone that contained a garnet (group II) and the core that included a cpx (unassigned).

Figure 3: a) Covariation of $\delta^{13}C$ and [N] measured in individual growth zones, subdivided in core (circle), intermediate (diamond) and rim (square). Coloured symbols are for dated growth zones of group I (red), group II (green), group III (purple), unassigned (dark blue) and undated zones (light blue). The data show a bi-modal distribution that is not observed in literature data (grey area) at Jwaneng

(Cartigny et al., 1998; Deines et al., 1997; Thomassot et al., 2009). b) Covariation in $\delta^{13}C$ and $\delta^{15}N$ analysed on polished fragments of six diamonds. Colour and symbols according to affiliated group colours and growth zones as in a).

Figure 4: Major element variation of inclusions: a) Molar Mg# versus Cr# for eclogitic high- and low-Cr cpx inclusions; fields for eclogitic and peridotitic paragenesis after Stachel & Harris (2008). Note: websteritic inclusions plot across in both E-/ P-type fields. b) Cr_2O_3 versus CaO (in wt.%) for garnet inclusions after Grütter et al. (2004) with distinction between high-/ low-Mg and high-Ca garnets. Jwaneng literature data from (Richardson et al., 1999; 2004) and Stachel et al. (2004).

Figure 5: REE_N patterns of a) Cpx inclusions with overall marked LREE enrichment. Inclusions of group I (red-shaded area) have a negative slope to sub-chondritic Lu (JW048, JW070, JW112, JW116, JW124). Inclusions of group II (green-shaded area) and unassigned (dark blue) show a broad range with $LREE_N$ enrichment (JW111, JW147) peaking at Pr–Sm with a gradual decrease in $MREE_N$ and $HREE_N$ to chondritic abundance in Lu. Other samples have complementary patterns with a depletion in Pr–Nd with flat $MREE_N$ and decreasing $HREE_N$ to chondritic Lu (JW137, JW138) or they have overall enriched but flat REE patterns decreasing to Lu (JW058). b) Garnets show either 'normal' $LREE_N$ depleted patterns (JW137, JW336) i.e., a steep positive slope within the $LREE_N$ and flat $MREE_N$–$HREE_N$ (with ~ chondritic abundance) similar to eclogitic garnet inclusions from diamonds worldwide (Stachel et al., 2004), or a negative slope in $MREE_N$–$HREE_N$ to sub-chondritic abundance (JW346, JW411), or $LREE_N$ depletion with increasing $MREE_N$ and flat $HREE_N$ (JW147) or slightly increasing to flat $LREE_N$ to $HREE_N$ patterns (JW058, JW355, JW450) with near-chondritic abundance.

Figure 6: a) Element distribution coefficients ($D_{REE}^{cpx/gnt}$) between garnet and cpx inclusions from the same diamond and for averages of all garnet and cpx inclusions from groups I to III compared to experimental data at 3 GPa/1400°C (Klemme et al., 2002), 4 GPa/1000°C (Kessel et al., 2005) and natural samples HRV247 and HRV313 (Harte & Kirkley, 1997). Note: JW147 cpx (core) and gnt (intermediate) are not in equilibrium resulting in a disrupted REE_N pattern; group I average is slightly

biased towards elevated REE contents due to the predominance of $LREE_N$ enriched cpx inclusions in this group. Group III average is based on undated cpx inclusions that were recovered from the same growth zone as the dated garnet inclusions in JW355 and JW450.

b) Reconstructed average whole rock REE patterns for inclusions of group I to III compared to N-MORB and a melt-depleted N-MORB residue (grey shaded area). All groups show enrichment in LREE and depletion in HREE. Worldwide average data and melt depletion curves are from Stachel et al. (2004).

Figure 7: a) Simplified W-E cross-section of the SCLM at Jwaneng with inferred tectonic setting. Eclogitic bodies (yellow) formed during the Archaean accretion of the Kaapvaal Craton. a) At ~ 1.8 Ga, amalgamation of the Kheis-Okwa-Magondi (K) and Rehoboth Terrain (R) to the Kaapvaal Craton was accompanied by subsequent extension and plutonism. The formation of group I diamonds coincided with the final stage of the assembly of the Proto-Kalahari Craton and occurred by large-scale (> 100's of km) metasomatism in a volatile-rich, fluid-dominated setting. B: Bushveld, M: Molopo Farms are related to the large igneous province at 2.05 Ga; G: Grunehogna Craton, eastern end of Proto-Kalahari. b) Successive accretion of Paleoproterozoic micro-continents (1.4 – 1.2 Ga) extended the Kalahari Craton to the west. At ~ 0.85 Ga, the breakup of the Rodinia supercontinent was accompanied by rifting and intra-plate magmatism along the NW and W margins of the Kalahari Craton. Diamonds of group II were formed by local re-mobilization and equilibration of different fluids in compositionally different eclogitic protoliths (enlargement) that had been incorporated into the SCLM over time.

Appendix

Appendix A: Analytical methods.

Table B.1: Uncorrected Rb-Sr and Sm-Nd isotope data of dated and undated eclogitic silicate inclusions from Jwaneng.

Table B.2: Carbon and nitrogen data of all analysed diamond growth zones from Jwaneng.

Table B.3: Major and trace element data of diamond inclusions together with properties of corresponding diamond host growth zones.

Table B.4: Total procedural blanks (tpb) of trace elements in [ppt] filtered for limit of quantification (LOQ).

Figure C.1: Representative diamonds with light microscope- & CL-images: FTIR traverses (white marker); $\delta^{13}C$ compositions of 'combustion' samples (light grey marker) and of 'SIMS' subdivided in traverses (black marker with stippled line) or measurements on polished fragments (black marker) together with their $\delta^{15}N$ values (dark grey) and derived N contents [at.ppm]; log [N] vs N aggregation [%B] for corresponding traverses to illustrate the potential thermal evolution across individual growth zones of a plate in reference to isotherms for theoretical mantle residence times of 2.66, 1.26 and 0.76 billion years that are based on inferred diamond formation ages at 1.0, 1.5 and 2.9 Ga, i.e., corrected for the 240 Ma kimberlite emplacement age. a) JW060: three distinct growth zones with $\delta^{13}C$ variations of up to 3‰ in the core indicating formation from different fluids; b) JW070 (group I): N is below detection limit, $\delta^{13}C$ shows limited variation(< 1.5‰), green slip lines indicate deformation; c) JW109: three distinct growth zones, $\delta^{13}C$ varies by < 1.5‰; d) JW112 (group I): N is below detection limit, $\delta^{13}C$ varies by < 2‰; e) JW137 (group II): resorption at the core-rim interface and deformation indicated in the rim, $\delta^{13}C$ varies by < 2‰; f) JW147: note the different characteristics of the intermediate zone that contained the garnet (group II) and the core that included the cpx (Unassigned); g) JW346 (group I): three distinct growth zones, $\delta^{13}C$ varies by 5‰ between rim and intermediate zone; h) JW355 (group III): the overall low N aggregation makes it difficult to clearly distinguish between core-rim.

Figure C.2: REE patterns of cpx inclusions that are undated in reference to coloured inclusions fields from group I (red), II (green) and III (purple) in the background; worldwide literature data as in Figure 5. Markers connected by solid lines represent inclusions that were recovered from the same growth zones that were dated using other inclusions from it, e.g., JW048, J070, JW124, JW137, JW411; stippled lines represent inclusions without any indication for ages.

Figure C.3: Theoretical parental REE fluid patterns of cpx and garnet inclusions using partitioning coefficients at 4 GPa/1000°C from Kessel et al. (2005). The fluids show a wide compositional range comparable to high density fluids trapped in fibrous diamonds from Jwaneng (Schrauder et al., 1996). The heterogeneity of group II melts illustrates the potential of different fluids precipitating diamonds at 0.85 Ga.